



HAL
open science

Linking sea level dynamic and exceptional events to large-scale atmospheric circulation variability: A case of the Seine Bay, France

Imen Turki, Nicolas Massei, Benoît B. Laignel

► To cite this version:

Imen Turki, Nicolas Massei, Benoît B. Laignel. Linking sea level dynamic and exceptional events to large-scale atmospheric circulation variability: A case of the Seine Bay, France. *Oceanologia*, 2019, 61 (3), pp.321-333. 10.1016/j.oceano.2019.01.003 . hal-02070404

HAL Id: hal-02070404

<https://normandie-univ.hal.science/hal-02070404>

Submitted on 16 Oct 2019

HAL is a multi-disciplinary open access archive for the deposit and dissemination of scientific research documents, whether they are published or not. The documents may come from teaching and research institutions in France or abroad, or from public or private research centers.

L'archive ouverte pluridisciplinaire **HAL**, est destinée au dépôt et à la diffusion de documents scientifiques de niveau recherche, publiés ou non, émanant des établissements d'enseignement et de recherche français ou étrangers, des laboratoires publics ou privés.



Available online at www.sciencedirect.com

ScienceDirect

journal homepage: www.journals.elsevier.com/oceanologia/



ORIGINAL RESEARCH ARTICLE

Linking sea level dynamic and exceptional events to large-scale atmospheric circulation variability: A case of the Seine Bay, France

Imen Turki*, Nicolas Massei, Benoit Laignel

Continental and Coastal Morphodynamic Laboratory, Normandy University, Rouen, France

Received 16 September 2018; accepted 15 January 2019

Available online 1 February 2019

KEYWORDS

Sea level dynamic;
Envelope approach;
Demodulated surges;
Storm events;
Climate patterns

Summary In this study, the multi-time-scale variability of the South English Channel (case of the Seine Bay, North France) sea level and its exceptional events have been investigated in relation with the global climate patterns by the use of wavelet multi-resolution decomposition techniques. The analysis has been focused on surges demodulating by an envelope approach. The low-frequency components of the interannual (2.1-yr, 4-yr, 7.8-yr) and the interdecadal (15.6-yr and 21.2-yr) time-scales, extracted from 46-years demodulated surges, have been correlated to 36 exceptional stormy events according to their intensity. Results have revealed five categories of storms function on their correlation with the interannual and the interdecadal demodulated surges: events with high energy are manifested at the full scales while moderate events are only observed at the interannual scales. The succession of storms is mainly carried by the last positive oscillations of the interannual and the interdecadal scales. A statistical downscaling approach integrating the discrete wavelet multi-resolution analysis for each time-scale has been used to investigate the connection between the local dynamic of surges and the global atmospheric circulation from SLP composites. This relation illustrates dipolar patterns of high-low pressures suggesting positive anomalies at the interdecadal scales of 15.6-yr and 21.3-yr and the interannual scales of 4-yr while negative anomalies at 7.8-yr should be related to a series of physical mechanisms linked to the North-Atlantic and ocean/atmospheric circulation oscillating at the same time-scales. The increasing storm frequency is probably related to the Gulf Stream variation and its weakening trend in the last years.

© 2019 Institute of Oceanology of the Polish Academy of Sciences. Production and hosting by Elsevier Sp. z o.o. This is an open access article under the CC BY-NC-ND license (<http://creativecommons.org/licenses/by-nc-nd/4.0/>).

* Corresponding author at: Continental and Coastal Morphodynamic Laboratory, Normandy University, Rouen 76821, France. Tel. +0033 235146952; fax: +0033 235140019.

E-mail addresses: imen.turki@univ-rouen.fr (I. Turki), nicolas.massei@univ-rouen.fr (N. Massei), benoit.laignel@univ-rouen.fr (B. Laignel). Peer review under the responsibility of Institute of Oceanology of the Polish Academy of Sciences.



1. Introduction

During the last decades and in relation with the global evolution induced by climate change, the oceanographic scientific community have devoted their efforts to improve our understanding of the impacts of climate fluctuations on coastal hydrodynamic variability, in particular during stormy events. Several approaches have been extensively employed to investigate the extreme physical dynamic of the sea level and simulate the impact of the global climate oscillations for providing different coastal projections. For this reason, determining how and to what extent the large-scale climate oscillations can be identified in the oceanographic parameters and storm surges is required.

In the present context of global changes, the combined effects of the sea level rise and the land loss are commonly mentioned as a consequence of climate variability (e.g., Devoy, 2008; Nicholls et al., 2010). In the same context, the land loss itself is often a result of an increasing storminess responsible for coastal erosion (Stive et al., 2002) or flooding areas whose repeated restoration might be inefficient and the land is abandoned.

The acceleration of the sea level rise along the coastal mid-Atlantic in recent decades, where the climate is strongly influenced by the Gulf Stream (GS), is possibly caused by the Atlantic Meridional Overturning Circulation (AMOC) and its upper branch, the GS. Consequently, coastal communities have observed a significant increase in flooding frequency in the last years (Mitchell et al., 2013).

By the hypothesis that the variation in the GS location and strength is responsible on changes in the sea surface height gradient across the GS and, consequently, the sea level variability on both sides of the stream, the elevation of the sea surface gradient is proportional to the surface velocity of the GS. Then, the weakening of the GS strength will raise the sea level northwest of the GS; which is suggested by several recent studies (e.g., Ezer and Corlett, 2012; Ezer et al., 2013; Levermann et al., 2005; Sallenger et al., 2012). The impact of the GS variation on coastal sea level has been demonstrated by many observations (Sweet et al., 2009) and circulations models (Ezer, 2001) of the Atlantic Oceans and, also, by Global Climate models (Yin et al., 2009).

The effects of continuous changes in atmospheric patterns on sea level dynamic and stormy events have been investigated through a series of probabilistic approaches based on climate indices by the use of nonstationary analyses of extremes (e.g. Miguez et al., 2012). Marcos et al. (2012) have related changes in the median and the higher-order percentiles of observed water levels in the Mediterranean Sea by the large-scale atmospheric circulation of winter North Atlantic Oscillation (NAO). Moreover, Menendez and Woodworth (2010) have demonstrated that changes in extreme events are due to changes in mean sea levels; they have reported the important role of the NAO and the Arctic Oscillation (AO) indices on the extreme sea level variability along the European coasts. Then, Masina et al. (2015) have shown a similar behavior between the regional and global scales at Venice and Porto Corsini (Adriatic Sea) from a detailed analysis of the annual mean sea level evolution. They have evidenced a relation between increasing extreme water levels since the 1990s and changes in wind regime, in

particular, the intensification of Bora and Sirocco winds events whose intensity and frequency have been increased after the second half of the 20th century.

One of the challenges in investigating the sea level dynamic with global patterns related to Climate circulation is how to identify the multi-scale variability associated with the different physical processes involved.

In the framework of the further altimetry mission of Surface Water and Ocean Topography (SWOT), planned for launch in 2021, Turki et al. (2015) have investigated the low-frequencies of the sea level variability in the eastern English Channel (NW France) at annual and inter-monthly scales. Such changes result from the combining effect of meteorological and oceanography forces with an important contribution of the hydrological signal coming from the Seine river; the climate signature of the NAO circulation is also observed at the annual scales. Massei et al. (2017) have focused on the relation of the local Seine hydrological variability with the global climate patterns, and the time-scale dependence of this connection by developing a downscaling modeling basing on an empirical statistical approach. Their works have shown that the multi-scale links between the sea level pressure (SLP) and the regional hydrological variations are statistically significant for frequencies greater than 2 years (3.2-yr, 7.2-yr and 19.3-yr); they should be caused by coupling effects of North-Atlantic oceanic paths and atmospheric circulation.

In this context, the present research has been carried out to investigate the multi-time-scale variability of the sea level in the Seine Bay (South English Channel) and its exceptional events in relation with the global climate patterns by the use of high-resolution spectral techniques. A special focus is devoted to the connection of stormy events and their occurrence with the atmospheric circulation. The paper is organized as follow. After the introduction, the second section presents the data and the methodological approach used. Section 3 provides all results and discussions of the multi-scale sea level variability in relation to the exceptional events and the teleconnections of the atmospheric circulation. Finally, some concluding remarks and further researches are presented in Section 4.

2. Data and methodological approach

2.1. Sea level and climatological data set

Hourly sea level measurements, extracted from Le Havre tide gauge between 1964 and 2010, have been provided by the National Navy Hydrographic Service (<http://refmar.shom.fr/en/home>); see Fig. 1. Climatological data in the North Atlantic zone have been extracted from the National Center for Environmental Prediction and National Center for Atmospheric Research-1 (NCEP/NCAR-1) reanalysis (Kalnay et al., 1996) with a time resolution of a month. This dataset represents the North Atlantic atmospheric dynamics over the North Atlantic region (75°W–35°E and 15°E–75°N) with a horizontal spatial resolution of 2.5*2.5 (i.e., 1125 grid-points). As suggested by previous researches, SLP field is considered as a good indicator for the local hydro-climatic conditions (e.g., Massei et al., 2017; Ruiger and Golian, 2015); it has been used in the present analysis and will be

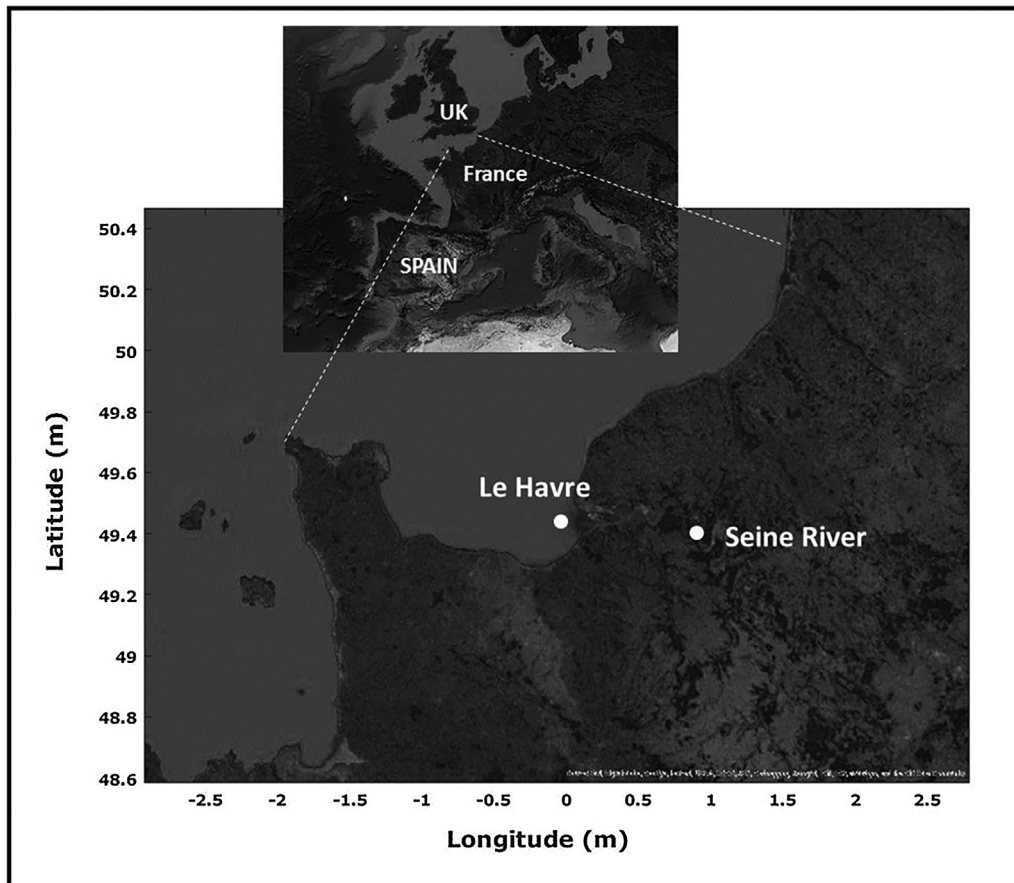


Figure 1 Study area: the Seine Bay located in the south-eastern English Channel (NW France).

referred to “large scale” in the subsequent parts of the analysis while local scale” refers to the sea level.

2.2. Tidal modulation and residual sea level

The total sea level height, resulting from the astronomical and the meteorological processes, exhibits a temporal non-stationarity explained by the combining effects of the long-term trend in the mean sea level, the modulation by the deterministic tidal component and the stochastic signal of surges, and the interactions between tides and surges. The occurrence of extreme sea levels is controlled by periods of high astronomically generated tides, in particular at inter-annual scales when two phenomena of precession cause systematic variation of high tides. The modulation of tides contributes to the enhanced risk of coastal flooding.

The separation between tidal and non-tidal signals is an important task in any analysis of sea level timeseries. The stochastic component associated with the non-tidal variation in the Seine Bay, extracted from Le Havre tide gauge, is mainly explained by the meteorological and the hydrological effects of the Seine river reaching the bay during flood events. By the hypothesis of independence between the astronomical and the stochastic effects, the non-linear relationship between both components is not considered to separate the tidal modulation from the total sea level.

Using the classical harmonic analysis, the tidal component has been modeled as the sum of a finite set of sinusoids at

specific frequencies to determine the determinist phase/amplitude of each sinusoid and predict the astronomical component of tides. In order to obtain a quantitative assessment of the non-tidal contribution in storminess changes, technical methods basing on MATLAB t-tide package have been used to estimate year-by-year tidal constituents. The sea level measurements present strong tidal modulations which have long been recognized by their significant effects on long-term changes (e.g., Gratiot et al., 2008); in particular, those produced at inter-annual scales. These processes result from 18.61-year lunar nodal cycle and the 8.85-year cycle of lunar perigee and influence the sea level as a quasi 4.4-year cycle (Menendez and Woodworth, 2010; Wood, 2001; Woodworth and Blackman, 2004).

A year-by-year tidal simulation (Shaw and Tsimplis, 2010) has been applied to the sea level timeseries to determine the amplitude and the phase of tidal modulations using harmonic analysis fitted to 18.61, 9.305, 8.85, and 4.425-year sinusoidal signals (Pugh, 1987).

2.3. Demodulated surges by the use of envelope technique

Once the annual sea level trend and the tidal components have been removed, the residual signal has been used as ‘surges’ to be demodulated by an envelope approach, a preliminary step before the frequency decomposition by the multi-resolution wavelet.

Determining envelopes of a statistical signal is generally used for detecting the amplitude modulation. In the present research, the objective is to detect if any (and what) underlying low-frequency component controls the variations of the sea level signal amplitude. The most known envelope is the analytic one based on the Hilbert transform. However and in practice, calculating envelopes of real signals in environmental contexts is different from analytic ones, although these uniquely define envelopes (Yang, 2017). The most methods for envelope identification depend on extrema detection followed by a low-pass filter. The envelopes of real signals are obtained using a spline interpolation from extrema sequences, as used for instance in the empirical mode decomposition (EMD) (Massei and Fournier, 2012; Massei et al., 2017). Here, the present work is more particularly interested in high surges with extreme values from considering only the upper envelope of a real-valued surge signal by identifying all the local maxima and interpolating between them using a cubic spline.

2.4. Atmospheric composite maps

The relationship between the local sea level variability and the global atmospheric patterns has been investigated to identify the physical links at different time-scales by the use of the Sea Level Pressure (SLP) field. The procedure for investigating this global/local scale connection consists in decomposing both the SLP field and the surge signal across the different time-scales into a series of wavelet details (WD) using a multiresolution analysis.

Then, for each wavelet time-scale, an associated SLP composite map is constructed by: (1) calculating the

point-wise (i.e. at each grid-point) positive temporal mean of the SLP field WD at this scale for high values of the corresponding surge WD, (2) similarly, calculate the point-wise negative temporal mean of SLP field WD for low values of surge WD, (3) computing the difference positive mean-negative mean SLP value at each grid point (Massei et al., 2017). Here, “high” and “low” values of sea level WD have been chosen such as they exceed $+0.5$ or fall below -0.5 standard deviation (SD). Statistically significant regions have been estimated for each wavelet scale from the highest to the lowest frequencies; the degrees of freedom has been adjusted according to the wavelet scale and the “effective” sample size N from the actual sample size N has been calculated according to the first order autocorrelation coefficient $AR[1]$ of each of the two positive and negative mean SLP WD (Mitchell et al., 1966).

3. Results and discussions

3.1. Sea level dynamic and exceptional events in the Seine Bay

The sea level variability in the Seine Bay has been investigated from the 46-year record. Once the tidal components and the regressive trend of the sea level rise were removed, the signal of surges has been demodulated by an envelope approach; then, the upper envelope has been calculated by joining local extrema and using a spline function (Fig. 2a).

Taking the Fourier transform of the original and the demodulated surges, the spectrums S_S and S_{SM} have been simulated in Fig. 2b with the aim to illustrate the different frequency components characterizing each signal. Compar-

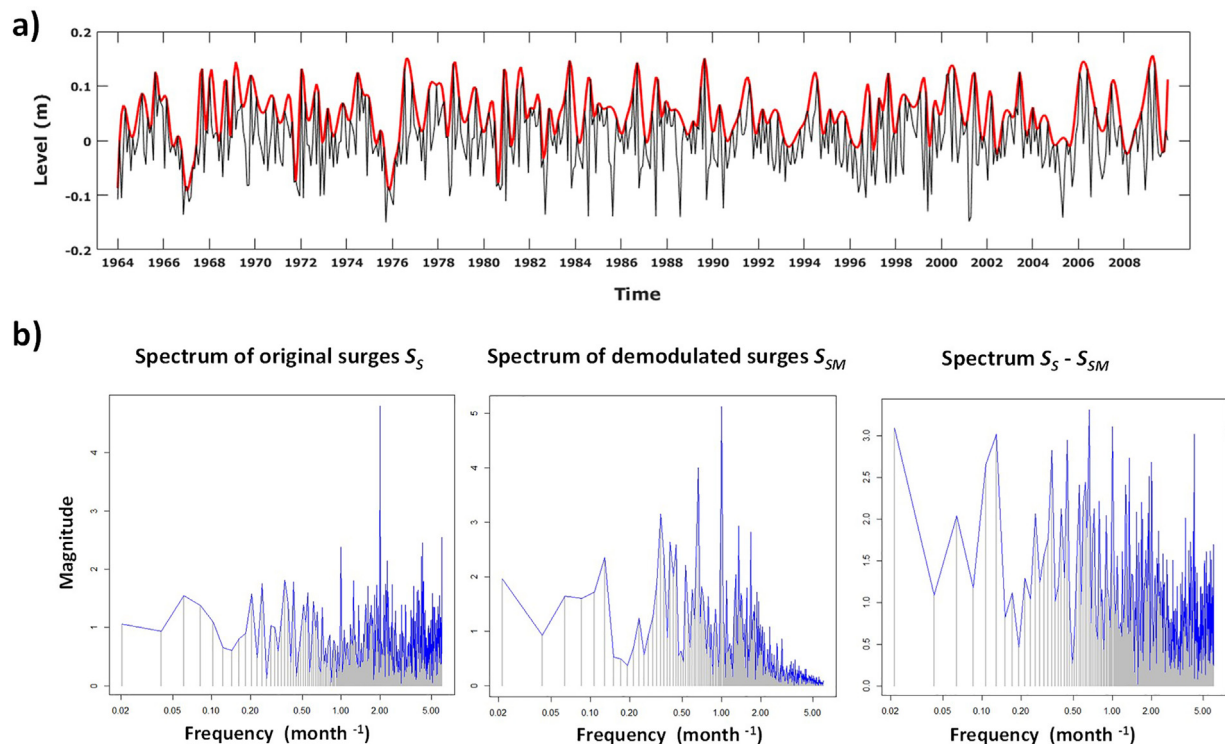


Figure 2 (a) The maxima envelope (thick line) of the mean monthly surges (thin line) between 1961 and 2010; (b) spectrum of the original S_S , demodulated S_{SM} surges, and the difference $S_S - S_{SM}$.

ing both spectrums shows that the interpolative envelope contains the message signal of the original surges: similarities of the main components with the most vibration of the high-frequency components in the original signal vs a clear illustration of low-frequency components in the demodulated signal. Hence, the simulated upper envelope can be used to modulate the main information of nonstationary surges.

The interpolative envelope, used for demodulating nonstationary surges, contains the lower chirp signal component with the fault characteristic frequency and its harmonic interferences. The demodulated surges cover a series of frequencies with different time-periods able to reconstruct the most variability of the original signal. This result confirms the last investigations reported by Yang (2017); they have concluded that the envelopes of real-valued stationary and nonstationary signals contain some low-frequency components of the original signal and some new components generated by the new-Nyquist extrema sampling.

Fig. 3 displays the continuous wavelet spectrum of the total sea level (a), surges (b) and the demodulated surges (c). The first spectrum (Fig. 3a) shows that most of the energy is homogeneously located around 1-yr with more than 90% of the total variance. By removing the astronomical components, the signal of surges reveals the existence of frequencies lower than 1-yr, differently distributed at 2-yr and 4-yr scales; it illustrates a non-homogeneous repartition during the period 1964–2010 (Fig. 3b) with two peaks of energy in both periods 1970–1980 and 2000–2001. The 2-yr and 4-yr frequencies are even more pronounced in the spectrum of the demodulated surges where the interannual and the interdecadal frequencies of 8-yr and 15-yr, respectively, are clearly structured with a high concentration of energy (Fig. 3c).

A multiresolution analysis has been applied to the demodulated surges with the aim to extract the different components explaining the total variability of the envelope. The process has resulted in the separation of 9 components, the so-called wavelet details numbered from D1 to D9.

The different wavelet details have been associated to the following time-scales: intermonthly (D1, D2 and D3), annual (D4), interannual (D5, D6 and D7) and interdecadal (D8 and D9) scales. The most part of these frequencies has been illustrated as peaks of energy in the continuous wavelet spectrum (Fig. 3c).

The focus of the present research is to investigate the key role of the low-frequency components (higher than 2-yr) with a mean explaining variance of 82.7% from the total demodulated signal (Table 1): ~ 2.1 -yr, ~ 4 -yr, ~ 7.8 -yr, ~ 15.6 -yr and ~ 21.3 -yr. This distribution of variance between 2-yr and 21-yr implies the importance of the large-scale variability in surges of the Seine Bay.

Similar scales, reported by Massei et al. (2017) from Seine watershed precipitations, have only presented a mean explained variance of 30% showing a low contribution of the large-scales in the total energy of the signal and highlighting the eventual weak dependence between high and low frequencies. In the case of high discrepancies between the different frequencies composing some statistical signals and with the aim to extract their low-frequency components, demodulating their evolution by the use of the envelope technique should be a useful way to investigate more deeply their large-scale behavior.

A total of 36 exceptional stormy events (from E_1 to E_{36}) produced in the Seine bay during the period 1964–2010 and with surges higher than 2-yr return period level has been extracted from REFMAR data base (Table 2). The different storms have been reported to the low-frequency components of the demodulated surges by vertical color bars (Fig. 4).

Five categories have been defined and attributed to the different storms according to their surge return period (Re): “A” with $Re = 2$ -yr, “B” 2 -yr $< Re < 5$ -yr, “C” with 5 -yr $< Re < 10$ -yr, “D” with 10 -yr $< Re < 20$ -yr and “E” with $Re > 20$ -y using gray, yellow, red, purple and dark purple colors, respectively. The closing events succeeding in time within a given period (days to months) are represented in Fig. 4 by only one vertical bar whose color is attributed to the higher category of storms produced during this period.

The first two categories of storms with a moderate surge return period are related to higher frequencies and can be observed at scales smaller than ~ 4 -yr. For example, stormy events E_8 , E_{16} and E_{17-19} of the category “A” (gray box in Fig. 4) are mainly manifested at 2.1-yr and seem to be not expressed at higher scales. E_{3-7} , E_{9-10} and E_{32-34} of the category “B” (yellow box in Fig. 4) are well observed at the interannual scales 2.1-yr and 4-yr. The events E_1 , E_{11} , E_{20-21} , E_{35} and E_{36} of the category “C” (red box in Fig. 4) are manifested at the three scales 2.1-yr, 4-yr and 7.8-yr. The category “E”, E_{13} , E_{28-29} and E_{30-31} (dark purple box in Fig. 4),

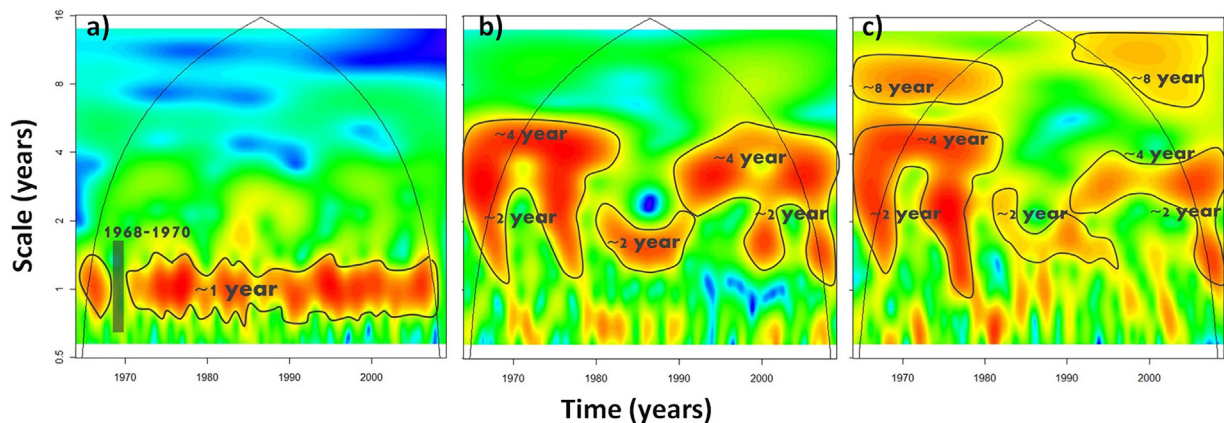


Figure 3 Continuous wavelet diagram of the monthly mean sea level: (a) the total sea level, (b) the surges and (c) the demodulated surges (maxima envelope) between 1964 and 2010.

Table 1 Equivalent Fourier period, standard deviation and energy, expressed as the percentage of total standard deviation of the maxima envelope, associated with each component (i.e. wavelet details and smooth) of Seine surges between 1964 and 2010.

Surges	D1–D4	D5	D6	D7	D8	D9	Total
Fourier period (yr)	$\leq \sim 1$	~ 2.1	~ 4	~ 7.8	~ 15.6	~ 21.3	–
Standard deviation (m)	0.01	0.009	0.005	0.0035	0.003	0.005	–
Energy (%)	17.3	32	26	11	8	5.7	100

is fully manifested at the different time-scales while E_2 , E_{14-15} and E_{23-27} of the category “D” (purple box in Fig. 4) pass away the lowest frequency of 21.1-yr.

According to this analysis, 36 high stormy events ($Re > 2$ -yr) have been identified during a period of 46 years; they are of different categories depending on the surge return period and the time-scale associated with the spectral period: 19 events of category “A” with 2.1-yr, 6 events of category “B” with 4-yr, 5 events of category “C” with 7.8-yr, 3 events

of each category “D” and “E” with 15.6-yr and 21.3-yr, respectively.

The distribution of storms is not homogeneous in time and their occurrence according to the different categories takes a nonstationary behavior since the number of events in a window of one-year changes in time. Results have shown that 24 among 46 years do not display any significant event ($Re > 2$ -yr) emphasizing alternating phases of moderate energy and storminess. Moderate phases with non-significant

Table 2 List of stormy events produced between 1964 and 2010; only storms with surge return period (Re) higher than 2 years.

Number of event	Date of event	Return period of surges (Re)	Tidal cycle
E_1	20 January 1965	5–10 years	Spring tide (coefficient 102)
E_2	27 November 1965	10–20 years	Neap tide (coefficient 68)
E_3	11 March 1967	2 years	Neap tide (coefficient 86)
E_4	04 October 1967	2–5 years	Spring tide (coefficient 113)
E_5	13 November 1967	2 years	Neap tide (coefficient 63)
E_6	02 November 1967	2–5 years	Spring tide (coefficient 111)
E_7	07 January 1968	2 years	Neap tide (coefficient 50)
E_8	06 July 1969	2 years	Neap tide (coefficient 67)
E_9	06 February 1974	2 years	Spring tide (coefficient)
E_{10}	09 February 1974	2–5 years	Spring tide (coefficient 112)
E_{11}	25 December 1976	2–5 years	Neap tide (coefficient 70)
E_{12}	15 December 1979	2 years	Neap tide (coefficient 66)
E_{13}	13 December 1981	>20 years	Spring tide (coefficient 104)
E_{14}	25 October 1984	2 years	Spring tide (coefficient 100)
E_{15}	22 November 1984	10–20 years	Spring tide (coefficient 102)
E_{16}	15 October 1987	2 years	Neap tide (coefficient 28)
E_{17}	20 December 1989	2 years	Neap tide (coefficient 90)
E_{18}	03 January 1990	2 years	Spring tide (coefficient 103)
E_{19}	26 February 1990	2 years	Spring tide (coefficient 106)
E_{20}	20 January 1994	2–5 years	Neap tide (coefficient 50)
E_{21}	15 April 1994	5–10 years	Spring tide (coefficient 100)
E_{22}	19 February 1996	2 years	Spring tide (coefficient 113)
E_{23}	25 December 1999	10–20 years	Spring tide (coefficient 104)
E_{24}	22 January 2000	5–10 years	Spring tide (coefficient 106)
E_{25}	08 February 2000	2 years	Neap tide (coefficient 88)
E_{26}	04 April 2000	2 years	Spring tide (coefficient 98)
E_{27}	02 September 2000	2 years	Spring tide (coefficient 94)
E_{28}	10 October 2000	>20 years	Spring tide (coefficient 101)
E_{29}	29 October 2000	2 years	Spring tide (coefficient 95)
E_{30}	17 September 2001	>20 years	Spring tide (coefficient 115)
E_{31}	28 December 2001	2 years	Neap tide (coefficient 74)
E_{32}	08 February 2004	2 years	Spring tide (coefficient 90)
E_{33}	10 December 2004	2 years	Neap tide (coefficient 79)
E_{34}	08 April 2005	2–5 years	Spring tide (coefficient 104)
E_{35}	11 March 2008	5–10 years	Spring tide (coefficient 106)
E_{36}	09 January 2009	5–10 years	Spring tide (coefficient 108)

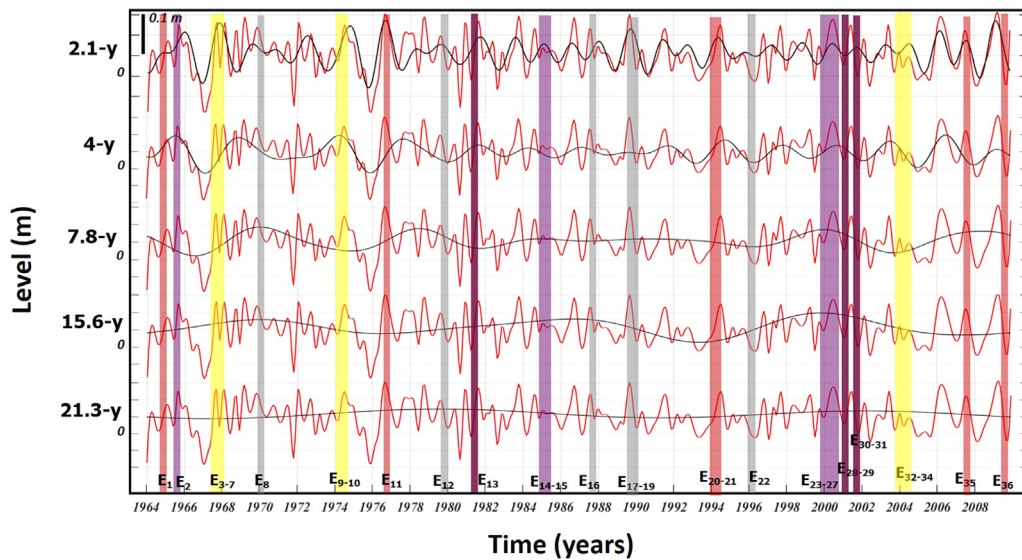


Figure 4 Multiresolution decomposition of the monthly surges, using the so-called, redundant, maximum-overlap discrete wavelet transform. Wavelet detail at scales higher than 1 year: 2.1-yr, 4-yr, 7.8-yr, 15.6-yr and 21.3-yr. The 36 exceptional stormy events with different categories function of their return period (R_e), occurred during the period 1964–2010, are illustrated by colored boxes: “A” (gray line) $R_e = 2$ -yr, “B” (yellow line) $2\text{-yr} < R_e < 5$ -yr, “C” (red line) $5\text{-yr} < R_e < 10$ -yr, “D” (purple line) $10\text{-yr} < R_e < 20$ -yr and “E” (dark purple line) > 20 -yr.

storms are longer with 3–4 successive years during the first 35 years (1964–2000) and decrease to 2 years in the beginning of the last decade when the succession of events seems to be more important. Stormy phases display different categories of events mainly distributed between November and February with only 11% of storms observed in October. Some events for each of September (2000, 2001), April (1994 and 2000) and March (1967 and 2008), July (1967) have been associated with the category “A”.

This connection between the low-frequency components and the historical record of the exceptional events suggests that storms would occur differently according to a series of physical processes oscillating at multi-time-scales; these processes control their frequency and their intensity.

The seasonal dependence between stormy events and the extreme sea levels, already observed in previous works (e.g., Tsimplis and Woodworth, 1994), is mainly caused by astronomical forces of spring tides and meteorological conditions of seasonal storms. This dependence explains the distribution of storms and their organization in time; which is strongly related to the large-scale variability of surges. For example, the four storms of 1967 (E_3 to E_6) and the five storms of 2000 (E_{25} to E_{29}) show a seasonal dependence in their succession, tidal phase and intensity (return period).

The combining effect of local driven forces with meteorological, oceanographic and hydrological origins explains the most significant of the stochastic signal of surges in the Seine Bay where the fluvial activity plays an important role in changes of water elevations. This activity is largely observed during flooding periods; an example is produced in December 2001 (e.g., Massei and Fournier, 2012) when E_{31} of the category A has occurred.

The origin of physical processes responsible for storm surges exhibits a temporal nonstationary behavior due to a

combination between the seasonal, the interannual and the interdecadal variability, and a non-linear interaction between the different time-scales. The assessment of the nonstationary effect on the estimation of extreme surges should be largely considered in the methods of extreme analysis by the use of the nonstationary models. For example, a time-dependent Generalized Extreme Value (GEV) distribution has been used by Masina and Lamberti (2013) to model the nonstationary features contained in the sea level time series by introducing the seasonality effect of GEV parameters (location, scale and shape) in order to improve the fitting of extreme values and reduce the uncertainty on the estimation of the return levels.

3.2. Relationship between storm surge dynamics and the atmospheric patterns

This section is focused on the connection between the local large-scale variability of surges and the global climate changes induced by the atmospheric circulation.

The climate patterns, extensively studied over the last two decades, have been mainly described by the NAO mechanisms (e.g. Hurrell et al., 2003). The SLP fields covering the English Channel, between 1964 and 2010, have been used with their different structures to characterize the climate patterns from the wavelet multiresolution decomposition into different time-scales.

Five composite maps have been calculated from the SLP field and the large-scale components of demodulated surges (Fig. 5). Provided maps are focused only on low frequencies ranging between 2.1-yr (D5) and 21.3-yr (D9) whose fluctuations correspond to oscillations periods less than half the length of the time series, and with the high-energy contribution on the variance of the total signal. As suggested by these

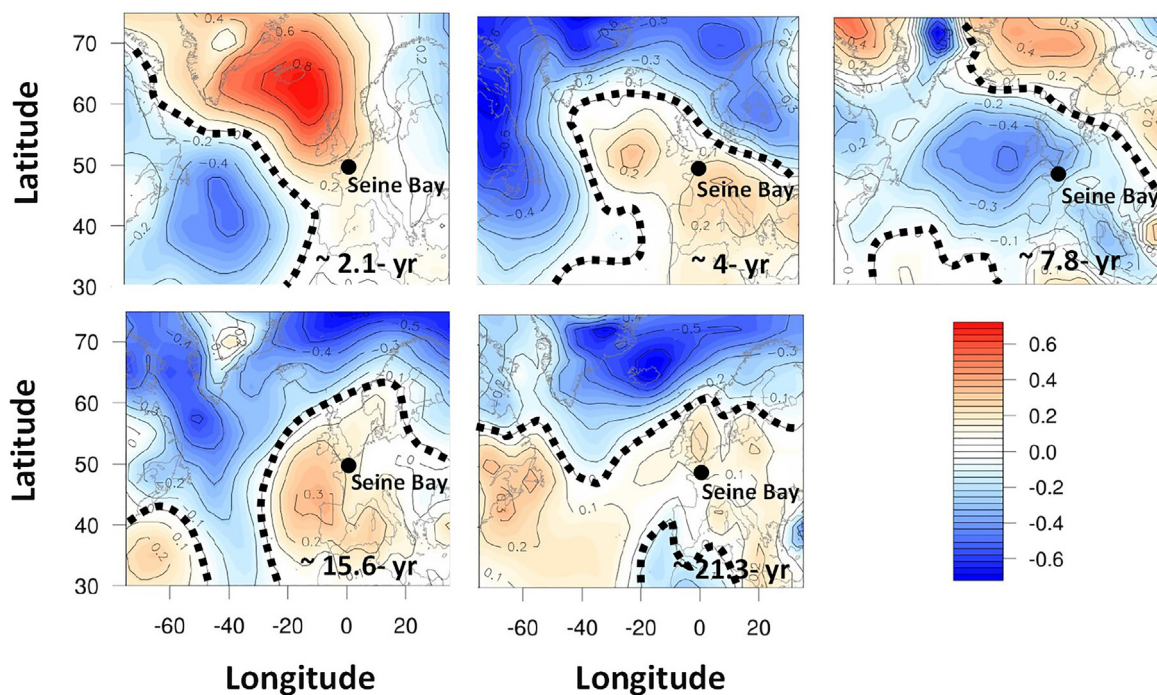


Figure 5 Composite maps of SLP generated for each scale based on surge variability. Black dashed lines indicate statistically significant regions (Student *t*-test with a 95% confidence limit).

composite maps, the relationship between the demodulated surges and the SLP fields is statistically significant and varies spatially in magnitude and phase. The spatial extent and the location of high-low pressure regions displayed by the atmospheric patterns are organized differently according to the time-scales of variability. Both 2.1-yr and 7.8-yr time-scales have shown dipolar structures with high-pressure anomalies located over the northern North Atlantic/sub-Arctic regions and low-pressure anomalies across the Atlantic (2.1-yr time-scale) and developing toward the English Channel and the North Sea (7.8-yr time-scale). Such dipolar structures can be associated with the typical western circulation, reminiscent of the negative NAO regime, more particularly for the 7.8-yr time-scale. This distribution should be attributed to the cyclonic circulation over northwestern Europe (50°N) with an alternating increase and decrease of West moisture fluxes from the Atlantic Ocean to the southern side of the English Channel and the Seine Bay.

On the contrary, 4-yr (D6), 15.6-yr (D8) and 21.3-yr (D9) time-scales have pointed North-South structures that could not be related to western circulation. Trough-shaped SLP anomalies in the center of the North-Atlantic basin would suggest weakened western circulation dynamics that would not be preeminent at these time-scales. In their analysis of multi-time-scale hydroclimate dynamics over the Seine river watersheds in Northern France, [Massei et al. \(2017\)](#) have found similar pattern shapes of SLP composites calculated from the Seine rainfall at the same time-scales.

Similar low-frequency oscillations have also been outlined by [Feliks et al., 2011](#) in relation with NAO patterns of the simulated marine atmospheric boundary layer (MABL) forced with SST from a simple Ocean Data Analysis. Such relations to

NAO index have been also observed by [Turki et al. \(2015\)](#) from the sea level fluctuations for scales between 1-yr and 3-yr, while the origin of higher frequencies, smaller than 1-yr, is related to the seasonal cycle of alternating high-low energy and changes in river discharges and temperature.

The different time-scales of the local variability of surges is not linearly related to the atmospheric circulation processes since their spatial extent, highlighted by the wavelet-based composite analysis, seems to be not fully similar according to the different scales of the hydro-climatic variability; each time-scale is associated with a determined physical mechanism explaining the oscillation period of changes.

The “switch on” and “off” of the influence of climate patterns on the variability of surges have an important application for many predictability issues. In this way, if SLP structures and surges anomalies are of similar patterns, the use of surges for predicting its variability from the SLP patterns at different time-scales could increase the accuracy of statistical predictions. At these scales, the atmospheric teleconnections explained by a series of physical mechanisms show a nonstationary behavior with a focus in the stochastic variability of surges.

This behavior is still under debate ([Martin-Rey et al., 2012](#); [Polo et al., 2008](#); [Rodriguez-Fonseca et al., 2009](#)).

According to their works related to the nonstationarities of the Atlantic influence on the Pacific in the 20th century, [Lopez-parages et al. \(2013\)](#) have shown that the statistical predictability of the rainfall variability can be improved by selecting the most suitable predictors depending on the period on which the prediction is carried out. They have also suggested that the nonstationary link between rainfall and SST takes place when the dipolar patterns of rainfall is

reinforced and coincides with negative phases of the AMO (Atlantic Multidecadal Oscillation) index along the 20th century.

Hence, the results obtained here point out a nonstationary behavior of the teleconnections between the local surges and the global SLP field, in particular for the interannual oscillations modulated by the interdecadal scales. The physical coherent modulation at a multi-scale variability is mainly related to the atmospheric circulation influenced generally by ocean currents and the Gulf Stream (GS). Several questions behind the reasons for this nonstationary teleconnections remain open, as the origin of the modulating factors.

In fact, the sea level pressure (SLP) and the baroclinic instability of wind stress are related to the GS path as given by NCEP reanalysis. In fact, the dominant signal is a northward (southward) displacement of the GS after the NAO reaches positive (negative) extrema (Frankignoul et al., 2001).

In the present context of global changes, the underlying issue of rising sea levels is combined to more stormy events and extremes. The increasing trend of stormy events in the Seine Bay, probably induced by the sea level rise scenarios of the English Channel, should be highly correlated with large variations in the GS transport (Ezer et al., 2013). The hypothesis of the GS transport reduction resulting in slower surface geostrophic currents, smaller gradients across the GS, and higher variations in the coastal sea level in the north GS has been supported by global climate models and satellite observations. Ezer et al. (2013) have demonstrated a strong relation between the coastal sea level changes and the GS variations on time-scales ranging from a few months to many decades with an increasing explained variance. The shift of the GS from 6–8 year oscillation cycle to a continuous weakening trend since the beginning the last century; which corresponds to the period of changes in storm organization and an increase in their frequency in time.

4. Conclusions

This research is focused on investigating the nonstationary dynamic of surges in the Seine Bay (southern side of the English Channel, NW France) and its nonlinear relationship with the global atmospheric circulation basing on a spectral approach of wavelet multi-resolution decomposition. By the use a new technique of envelope for demodulating surges, the large-scale variability has been quantified during 46 years (1964–2010). A total of 36 exceptional stormy events has been reported to the interannual (2.1-yr, 4-yr and 7.8-yr) and interdecadal (15.6-yr and 21.3-yr) time-scales of surges. Results have suggested a strong connection between the categories of storms, their intensity (return period 'Re') and their organization in time with the large-scale variability of surges. In fact, the interannual scales of 15.6-yr and 21.3-yr have been linked to stormy events with Re higher than 10 years; storms with Re of 2 years are only manifested at 2.1-yr scales, while events with Re between 2 and 10 years have been reported to 4-yr and 7.8-yr scales. Dipolar patterns of high-low pressures have been detected at 2.1-yr and 7.8-yr scales and should be related to the western circulation having an impact on the sea surge maxima, while the variability of 4-yr, 15.6-yr and 21.3-yr should obey to different mechanisms related to the pronounced North-South circula-

tion processes and NAO, as interpreted from the distribution of SLP anomalies.

The present investigation brings some interesting results about the nonstationary behavior the teleconnections between the local surges and the global climate circulation at large-time scales. By simulating the low-frequency components of demodulated surges and SLP fields, results have highlighted the important role of the interdecadal frequencies in the modulation of interannual variability. Deeper investigations related to the physical mechanisms responsible for this nonstationary dynamic are required in order to improve our understanding of the system climate-ocean changes.

The conclusion of this research suggests that wind–stress variations driven by energetic currents such as the GS may play a key role in coastal sea level changes. Establishing a strong connection between large-scale sea level changes with flooding risks and the GS gradients could improve our understanding of the relation between the global climate patterns and the local sea level changes; also allow us to infer the future projections of sea level change and extreme events.

This finding can represent a step forward in the understanding of the role of the sea level surges and should be useful to improve the downscaling models of sea surges, therefore allowing a better assessment of flood risks. Further works will be focused on developing the large-scale/local-scale nonstationary models by the use of different large-scale variables related to the atmospheric circulation. This may allow proposing the improved statistical downscaling models and exploring the capabilities of such models to produce forecasts of the probability of extreme sea level trends by considering the interannual and the interdecadal variability of global climate patterns.

Acknowledgments

The authors are grateful to ANR funded project “RICCOCHET” of French national program as well as the international project COTEST funded by CNES-TOSCA and related to the future mission of Surface Water and Ocean Topography (SWOT). Authors thank also National Navy Hydrographic Service and National Center for Environmental Prediction for providing sea level and atmospheric data. Also, the authors greatly thank the reviewers and the editors of the journal *Oceanologia* for their useful suggestions to improve the manuscript.

References

- Devoy, R.J.N., 2008. Coastal vulnerability and the implications of sea level rise for Ireland. *J. Coast. Res.* 24 (2), 325–341, <http://dx.doi.org/10.2112/07A-0007.1>.
- Ezer, T., 2001. Can long-term variability in the Gulf Stream transport be inferred from sea level? *Geophys. Res. Lett.* 28 (6), 1031–1034, <http://dx.doi.org/10.1029/2000GL011640>.
- Ezer, T., Atkinson, L.P., Corlett, W.B., Blanco, J.L., 2013. Gulf Stream's induced sea level rise and variability along the U.S. mid-Atlantic coast. *J. Geophys. Res.* 118, 685–697, <http://dx.doi.org/10.1002/jgrc.20091>.
- Ezer, T., Corlett, W.B., 2012. Analysis of relative sea level variations and trends in the Chesapeake Bay: is there evidence for accelera-

- ation in sea level rise? In: Proc Oceans'12 MTS/IEEE, October 14–19, IEEE Xplore, <http://dx.doi.org/10.1109/OCEANS.2012.6404794>.
- Feliks, Y., Ghil, M., Robertson, A.W., 2011. The atmospheric circulation over the North Atlantic as induced by the SST field. *J. Clim.* 24 (2), 522–542, <http://dx.doi.org/10.1175/2010JCLI3859.1>.
- Frankignoul, C., Coëtlogon, G., Joyce, T.M., Dong, S., 2001. Gulf Stream variability and ocean–atmosphere interactions. *J. Phys. Oceanogr.* 31 (12), 3516–3529, [http://dx.doi.org/10.1175/1520-0485\(2002\)031<3516:GSAVOA>2.0.CO;2](http://dx.doi.org/10.1175/1520-0485(2002)031<3516:GSAVOA>2.0.CO;2).
- Gratiot, N., Anthony, E.J., Gardel, A., Gaucherel, C., Proisy, C., Wells, J.T., 2008. Significant contribution of the 18.6 year tidal cycle to regional coastal changes. *Nat. Geosci.* 1 (3), 169–172, <http://dx.doi.org/10.1038/ngeo127>.
- Hurrell, J.W., Kushnir, Y., Ottersen, G., Visbeck, M., 2003. An Overview of the North Atlantic Oscillation. *Geophys. Monog. Ser.* 134, AGU, <http://dx.doi.org/10.1029/134GM01>.
- Kalnay, E., Kanamitsu, M., Kistler, R., Collins, W., Deaven, D., Gandin, L., Joseph, D., 1996. The NCEP/NCAR 40-year reanalysis project. *Bull. Am. Meteorol. Soc.* 77 (3), 437–472, [http://dx.doi.org/10.1175/1520-0477\(1996\)077<0437:TNYRP>2.0.CO;2](http://dx.doi.org/10.1175/1520-0477(1996)077<0437:TNYRP>2.0.CO;2).
- Levermann, A., Griesel, A., Hofmann, M., Montoya, M., Rahmstorf, S., 2005. Dynamic sea level changes following changes in the thermohaline circulation. *Clim. Dynam.* 24 (4), 347–354, <http://dx.doi.org/10.1007/s00382-004-0505-y>.
- Lopez-parages, J., Villamayor, J., Gomaeei, I., Losada, T., Martirey, M., Mohino, E., Polo, I., Rodriguez-Fonseca, B., Suarez, R., 2013. Nonstationary interannual teleconnections modulated by multidecadal variability. *Física de la Tierra* 25, 11–39, http://dx.doi.org/10.5209/rev_FITE.2013.v25.43433.
- Marcos, M., Chust, G., Jordá, G., Caballero, A., 2012. Effect of sea level extremes on the western Basque coast during the 21st century. *Clim. Res.* 51 (3), 237–248, <http://dx.doi.org/10.3354/cr01069>.
- Martin-Rey, M., Polo, I., Rodriguez-Fonseca, B., Kucharski, F., 2012. Changes in the interannual variability of the tropical Pacific as a response to an equatorial Atlantic forcing. *Sci. Mar.* 76 (S1), 105–116, <http://dx.doi.org/10.3989/scimar.03610.19A>.
- Masina, M., Lamberti, A., 2013. A nonstationary analysis for the Northern Adriatic extreme sea levels. *J. Geophys. Res.* 118, 3999–4016, <http://dx.doi.org/10.1002/jgrc.20313>.
- Masina, M., Lamberti, A., Archetti, R., 2015. Coastal flooding: a copula based approach for estimating the joint probability of water levels and waves. *Coast. Eng.* 97, 37–52, <http://dx.doi.org/10.1016/j.coastaleng.2014.12.010>.
- Massei, N., Dieppois, B., Hannah, D.M., Lavers, D.A., Fossa, M., Laignel, B., Debret, M., 2017. Multi time-scale hydroclimate dynamics of a regional watershed and links to large-scale atmospheric circulation: Application to the Seine river catchment, France. *J. Hydrol.* 546, 262–275, <http://dx.doi.org/10.1016/j.jhydrol.2017.01.008>.
- Massei, N., Fournier, M., 2012. Assessing the expression of large-scale climatic fluctuations in the hydrological variability of daily Seine river flow (France) between 1950 and 2008 using Hilbert-Huang Transform. *J. Hydrol.* 448–449, 119–128, <http://dx.doi.org/10.1016/j.jhydrol.2012.04.052>.
- Menendez, M., Woodworth, P.L., 2010. Changes in extreme high water levels based on a quasi-global tide-gauge data set. *J. Geophys. Res.* 115, C10011, <http://dx.doi.org/10.1029/2009JC005997>.
- Minguez, R., Tomas, A., Mendez, F.J., Medina, R., 2012. Mixed extreme wave climate model for reanalysis databases. *Stoch. Environ. Res. Risk. Assess.* 27, 757–768, <http://dx.doi.org/10.1007/s00477-012-0604-y>.
- Mitchell, J.M., Dzerdzeevskii Jr., Flohn, B., Hofmeyr, H., Lamb, W.L., Rao, H.H., Wallén, C.C., 1966. *Climatic change: Technical Note No. 79, report of a working group of the Commission for Climatology. WMO No. 195 TP 100.* World Meteorological Organization, Geneva, Switzerland, 81 pp.
- Mitchell, M., Hershner, C., Herman, J., Schatt, D., Eggington, E., Stiles, S., 2013. *Recurrent flooding study for Tidewater Virginia, Report SJR 76, 2012.* Virginia Instit. Marine Sci., Gloucester Point, VA, 141 pp.
- Nicholls, R., Brown, S., Hanson, S., Hinkel, J., 2010. *Economics of coastal zone adaptation to climate change, Discussion Paper 10.* World Bank, Washington, DC.
- Polo, I., Rodriguez-Fonseca, B., Losada, T., Garcia-Serrano, J., 2008. Tropical Atlantic variability modes (1979–2002). Part I: Time evolving SST modes related to West African rainfall. *J. Clim.* 21, 6457–6475, <http://dx.doi.org/10.1175/2008JCLI2607.1>.
- Pugh, D.J., 1987. *Tides, Surges and Mean Sea-Level: A Handbook for Engineers and Scientists.* John Wiley, Chichester, 472 pp.
- Rodriguez-Fonseca, B., Polo, I., Garcia-Serrano, J., Losada, T., Mohino, E., Mechoso, C.R., Kucharski, F., 2009. Are Atlantic Niños enhancing Pacific ENSO events in recent decades? *Geophys. Res. Lett.* 36, L20705, <http://dx.doi.org/10.1029/2009GL040048>.
- Ruigar, H., Golian, S., 2015. Prediction of precipitation in Golestan dam watershed using climate signals. *Theor. Appl. Climatol.* 123 (3–4), 671–682, <http://dx.doi.org/10.1007/s00704-015-1377-2>.
- Sallenger, A.H., Doran, K.S., Howd, P., 2012. Hotspot of accelerated sea-level rise on the Atlantic coast of North America. *Nat. Clim. Change* 2, 884–888, <http://dx.doi.org/10.1038/NCILMATE1597>.
- Shaw, A.G.P., Tsimplis, M.N., 2010. The 18.6 yr nodal modulation in the tides of Southern European Coasts. *Cont. Shelf Res.* 30 (2), 138–151, <http://dx.doi.org/10.1016/j.csr.2009.10.006>.
- Stive, M.J.F., Aarninkhof, S.G.J., Hamm, L., Hanson, H., Larson, M., Wijnberg, K.M., Nicholls, R.J., Capobianco, M., 2002. Variability of shore and shoreline evolution. *Coast. Eng.* 47 (2), 211–235, [http://dx.doi.org/10.1016/S0378-3839\(02\)00126-6](http://dx.doi.org/10.1016/S0378-3839(02)00126-6).
- Sweet, W., Zervas, C., Gill, S., 2009. *Elevated east coast sea level anomaly: June–July 2009, NOAA Tech. Rep. No. NOS CO-OPS 051.* NOAA NOS, Silver Spring, MD, 40 pp.
- Tsimplis, M.N., Woodworth, P.L., 1994. *The global distribution of the seasonal sea level cycle calculated from coastal tide gauge data.* *J. Geophys. Res.* 99 (C8), 16031–16039.
- Turki, I., Laignel, B., Chevalier, L., Costa, S., Massei, N., 2015. Coastal sea level changes in the southeastern side of the English channel: potentialities for future SWOT applicability. *IEEE J. Sel. Top. Appl. Earth Obs. Remote Sens.* 8 (4), 1564–1569, <http://dx.doi.org/10.1109/JSTARS.2015.2419693>.
- Wood, F., 2001. Tidal dynamics. Volume 1: theory and analysis of tidal forces. *J. Coast. Res.* 259–326, <https://www.jstor.org/stable/25736216>.
- Woodworth, P.L., Blackman, D.L., 2004. Evidence for systematic changes in extreme high waters since the mid-1970s. *J. Clim.* 17 (6), 1190–1197, [http://dx.doi.org/10.1175/1520-0477\(1996\)077<0437:TNYRP>2.0.CO;2](http://dx.doi.org/10.1175/1520-0477(1996)077<0437:TNYRP>2.0.CO;2).
- Yang, Y., 2017. A signal theoretic approach for envelope analysis of real-valued signals. *IEEE Access* 5, 5623–5630, <http://dx.doi.org/10.1109/ACCESS.2017.2688467>.
- Yin, J., Schlesinger, M.E., Stouffer, R.J., 2009. Model projections of rapid sea-level rise on the northeast coast of the United States. *Nat. Geosci.* 2, 262–266, <http://dx.doi.org/10.1038/NNGEO462>.